



ARL-TR-8964 • MAY 2020



Feasibility of Cryomilled 17-4 Stainless Steel Powder as Feedstock for Additive Manufacturing

by Frank Kellogg, Andelle Kudzal, Clara Mock, Josh Taggart-Scarff, Ryan Rogers, and Brandon McWilliams

Approved for public release; distribution is unlimited.

NOTICES

Disclaimers

The findings in this report are not to be construed as an official Department of the Army position unless so designated by other authorized documents.

Citation of manufacturer's or trade names does not constitute an official endorsement or approval of the use thereof.

Destroy this report when it is no longer needed. Do not return it to the originator.



Feasibility of Cryomilled 17-4 Stainless Steel Powder as Feedstock for Additive Manufacturing

Frank Kellogg, Clara Mock, and Josh Taggart-Scarff
SURVICE Engineering

Andelle Kudzal and Brandon McWilliams
Weapons and Materials Research Directorate, CCDC Army Research Laboratory

Ryan Rogers
Bennett Aerospace

REPORT DOCUMENTATION PAGE

Form Approved
OMB No. 0704-0188

Public reporting burden for this collection of information is estimated to average 1 hour per response, including the time for reviewing instructions, searching existing data sources, gathering and maintaining the data needed, and completing and reviewing the collection information. Send comments regarding this burden estimate or any other aspect of this collection of information, including suggestions for reducing the burden, to Department of Defense, Washington Headquarters Services, Directorate for Information Operations and Reports (0704-0188), 1215 Jefferson Davis Highway, Suite 1204, Arlington, VA 22202-4302. Respondents should be aware that notwithstanding any other provision of law, no person shall be subject to any penalty for failing to comply with a collection of information if it does not display a currently valid OMB control number.

PLEASE DO NOT RETURN YOUR FORM TO THE ABOVE ADDRESS.

| | | | | | |
|--|------------------------------------|---|---|--|--|
| 1. REPORT DATE (DD-MM-YYYY) May 2020 | | 2. REPORT TYPE Technical Report | | 3. DATES COVERED (From - To) 2 December 2018–1 May 2019 | |
| 4. TITLE AND SUBTITLE Feasibility of Cryomilled 17-4 Stainless Steel Powder as Feedstock for Additive Manufacturing | | | | 5a. CONTRACT NUMBER W911QX-16-D-0014 | |
| | | | | 5b. GRANT NUMBER | |
| | | | | 5c. PROGRAM ELEMENT NUMBER | |
| 6. AUTHOR(S) Frank Kellogg, Andelle Kudzal, Clara Mock, Josh Taggart-Scarff, Ryan Rogers, and Brandon McWilliams | | | | 5d. PROJECT NUMBER | |
| | | | | 5e. TASK NUMBER | |
| | | | | 5f. WORK UNIT NUMBER | |
| 7. PERFORMING ORGANIZATION NAME(S) AND ADDRESS(ES) CCDC Army Research Laboratory ATTN: FCDD-RLW-MD Aberdeen Proving Ground, MD 21005 | | | | 8. PERFORMING ORGANIZATION REPORT NUMBER ARL-TR-8964 | |
| 9. SPONSORING/MONITORING AGENCY NAME(S) AND ADDRESS(ES) | | | | 10. SPONSOR/MONITOR'S ACRONYM(S) | |
| | | | | 11. SPONSOR/MONITOR'S REPORT NUMBER(S) | |
| 12. DISTRIBUTION/AVAILABILITY STATEMENT Approved for public release; distribution is unlimited. | | | | | |
| 13. SUPPLEMENTARY NOTES ORCID IDs: Frank Kellogg, 0000-0003-3048-0255; Clara Mock, 0000-0001-8055-2371; Joshua Taggart-Scarff, 0000-0003-3540-7436 | | | | | |
| 14. ABSTRACT Additive manufacturing (AM) powder feedstock supplied by the manufacturer is often gas atomized and supplied without post-atomization treatment. By including a preprocessing treatment prior to AM, internal powder porosity could be reduced and grain size decreased, which could improve the AM process and the mechanical properties of the finished part. This study examined the feasibility of using cryomilling as a post-atomization powder treatment for laser powder bed fusion (L-PBF) AM feedstock, using gas atomized 17-4 stainless steel powder. The effect of cryomilling on powder characteristics, such as morphology and powder flow, and the influence on the L-PBF process was examined. As-built samples from the cryomilled powder were characterized through X-ray microcomputed tomography and optical microscopy. The as-built samples were porous due to the morphological changes to the powder induced by the cryomilling process. | | | | | |
| 15. SUBJECT TERMS cryomilling, additive manufacturing, laser powder bed fusion, powder feedstock, 17-4 stainless steel | | | | | |
| 16. SECURITY CLASSIFICATION OF: | | | 17. LIMITATION OF ABSTRACT UU | 18. NUMBER OF PAGES 24 | 19a. NAME OF RESPONSIBLE PERSON Frank Kellogg |
| a. REPORT Unclassified | b. ABSTRACT Unclassified | c. THIS PAGE Unclassified | | | 19b. TELEPHONE NUMBER (Include area code) (410) 306-0803 |

Contents

| | |
|---|-----------|
| List of Figures | iv |
| List of Tables | iv |
| Acknowledgments | v |
| 1. Introduction | 1 |
| 2. Experimental | 2 |
| 3. Results and Discussion | 3 |
| 4. Conclusion | 12 |
| 5. References | 14 |
| List of Symbols, Abbreviations, and Acronyms | 16 |
| Distribution List | 17 |

List of Figures

| | | |
|---------|--|----|
| Fig. 1 | SEM micrographs of the as-atomized powder. The circled regions show porosity in the powder, indicating hollow powder particles. | 3 |
| Fig. 2 | High-magnification micrographs in secondary a and b) and backscatter c and d) of the pore circled in Fig. 1c | 4 |
| Fig. 3 | Cross sections of powder samples showing a powder pore and hollow particle..... | 4 |
| Fig. 4 | Particle size distribution a) and sphericity b) measurements for the as-received powder | 5 |
| Fig. 5 | SEM micrographs: 2-h cryomilled powder a and b); 2-h cryomilled, degassed, and sieved powder c and d) | 6 |
| Fig. 6 | PSD a) and morphology measurements b) of the 2-h cryomilled powder and of the 2-h cryomilled, degassed, and sieved powder with the as-received powder | 6 |
| Fig. 7 | Schematic demonstrating the measurement limitations of the Camsizer, which would bias the sphericity results due to the morphological changes after cryomilling | 7 |
| Fig. 8 | XRD patterns of the 17-4 powders used in this study | 8 |
| Fig. 9 | TGA curve of stearic acid a) and DSC curves b) of the powders showing no difference between the thermal behaviors of the powders. c) Temperature regime over which stearic acid would be found. d) Melting and solidification portions of the curve. Exotherm up in b, c, and d with a 5 °C/min heating rate. | 8 |
| Fig. 10 | Brookfield powder flow results | 10 |
| Fig. 11 | Cylinders produced via L-PBF with cryomilled and degassed powder | 10 |
| Fig. 12 | μ CT slices along the build direction (length) of the cylinders | 11 |
| Fig. 13 | μ CT slices along the diameter (X-direction) of the cylinders | 11 |

List of Tables

| | | |
|---------|---|---|
| Table 1 | PSD and morphology measurements for the as-received, cryomilled, and cryomilled and degassed powders..... | 5 |
| Table 2 | Melting and solidification values from DSC measurements | 9 |

Acknowledgments

The research reported in this document was performed in connection with contract/instrument W911QX-16-D-0014 with the US Army Combat Capabilities Development Command (CCDC) Army Research Laboratory (ARL). The views and conclusions contained in this document are those of SURVICE Engineering, Bennett Aerospace, and the CCDC Army Research Laboratory. Citation of manufacturer's or trade names does not constitute an official endorsement or approval of the use thereof. The US Government is authorized to reproduce and distribute reprints for Government purposes notwithstanding any copyright notation hereon.

1. Introduction

Additive manufacturing (AM) is a catchall term for a suite of manufacturing processes that produces parts in a layer-by-layer method. Laser powder bed fusion (L-PBF) is an AM process by which layers of metallic powder are welded together by lasers to produce 3-D parts.¹⁻⁶ Powder feedstock for L-PBF is most often manufactured via gas atomization as this technique produces spherical powders with tailorable particle size distributions.²⁻⁶ Spherical powders provide the best combination of powder flow (enabling easy spreading for layer forming) and powder packing density (reducing porosity from poor powder layers).⁷⁻¹⁰ However, gas atomization can lead to nonspherical powders that may be hollow. It has been shown that hollow powders used during L-PBF can lead to increased porosity in the final part.²⁻⁵ The inert gas used for atomization can also play a role in the final microstructural phases that are present in the part, either creating a need to heat treat parts produced by L-PBF or compromised material properties.^{11,12}

A martensitic precipitation hardened stainless steel (SS), 17-4 PH SS, was chosen for this study because it is highly weldable. The weldability of 17-4 has shown the material to be easily adaptable to L-PBF and other AM processes, which has led it to being widely studied and used to produce parts. It is also a material that is very sensitive to the particular inert gas used during the atomization process. Atomization of 17-4 using argon produces powder with a martensitic grain structure while powder that was atomized using nitrogen leads to parts with large amounts of metastable austenite.^{11,12}

Cryomilling, in this study, is attrition ball milling in liquid nitrogen. Cryomilling has traditionally been used to produce nanostructured micron-sized powders for traditional powder metallurgy consolidation.^{13,14} In this study, 17-4 PH steel, atomized in argon, was cryomilled in liquid nitrogen for 2 h as a proof of concept to see if cryomilling could be used as a powder preprocessing method to improve the properties of the AM-produced parts. In these experiments nanostructuring is not the end goal, as any induced nanostructuring during cryomilling will be lost during the melting and solidification experienced during L-PBF. Instead, cryomilling is being used to remove any porosity that may be present in the initial powder. Cryomilling has also been shown to improve powder flow and sintering and may provide similar benefits to AM processing.¹⁵ The powder was only milled for 2 h to minimize incorporation of nitrogen via mechanical alloying during cryomilling.

2. Experimental

Commercially available argon gas atomized 17-4 SS powder (Carpenter Powder Products, Bridgeville, Pennsylvania) was used in this study. The as-atomized powder was characterized for particle size distribution (PSD) and morphology via a combination of scanning electron microscopy (SEM) (Hitachi S4700 FESEM) and dynamic image analysis (Retsch Camsizer X2). The microstructural phase of the powder was examined via X-ray diffraction (XRD) (Bruker D2 Phaser). Thermogravimetric analysis (TGA) and differential scanning calorimetry (DSC) (TA Instruments Q600) measurements were also used for phase investigation. Powder flow was measured using a Brookfield powder flow tester. These tests were run on the powder prior to cryomilling and after cryomilling and degassing. Degassing was necessary to remove stearic acid that had been blended with the powder prior to cryomilling. As a process control aid (PCA), 0.15 wt% of stearic acid was blended into 2 kg of 17-4 powder to inhibit cold welding during milling. The blending process was carried out with a Resodyn LabRAM II acoustic mixer operating for 1 h with 10 g's of acceleration.

Cryomilling was accomplished using a 32:1 media (1/4-inch diameter SS balls) to powder ratio at a mill speed of 300 rpm. The mill was filled with liquid nitrogen prior to powder addition. A sacrificial coating run using approximately 50 g of 17-4 powder was milled and discharged before adding the 2 kg of powder to prevent contamination from the mill and increase powder yield. After 2 h, the powder was discharged from the mill along with the liquid nitrogen into a large metal bucket that was immediately moved into a glovebox antechamber. The antechamber was cycled between vacuum and backfill (argon gas) until there were no noticeable pressure changes due to nitrogen boiling off. The bucket was then moved into the glovebox, under argon, until the remaining liquid nitrogen boiled off.

Inside the glovebox, the cryomilled powder was loaded and sealed in a reactor that was loaded into a rocking, fluidized bed furnace for degassing. Degassing was accomplished by heating the powder to 325 °C at 10 °C/min under flowing argon and holding it there for 6 h before cooling back to room temperature. After cooling, the reactor was removed, unloaded inside the glovebox, and the powder was sieved with a -325 mesh screen.

The powder was used as feedstock for L-PBF in a ProX DMP 100 from 3-D Systems using a laser power of 49 W, a scan speed of 140 mm/s, a hatch spacing of 0.07 mm, and a powder layer thickness of 0.03 mm. These parameters were developed from previous builds using as-atomized 17-4.¹ After L-PBF, the resultant cylinders were examined via X-ray microcomputed tomography (μ CT, Zeiss

Xradia 520 Versa) to provide a 3-D examination of the as-built parts. The entire part was scanned via μ CT with a 24- μ m voxel size at 140 kV and 72 μ A with an exposure time of 0.25 s and the 0.4 \times objective lens. Analysis of the scanned volume was conducted by thresholding of the pores through CTAn image processing software (Bruker microCT).

3. Results and Discussion

SEM micrographs of the as-atomized powders show that the powder particles match the -325 mesh size cut (particle diameters below 45 μ m) and while round, are not all perfect spheres and have a substantial amount of satellite particles (satellites are very small particles that decorate the surface of the primary particles, Fig. 1). A significant number of these particles have pores (Figs. 1 and 2). Powder cross sections were prepared by mounting the powders in resin and applying metallographic preparation techniques to prepare a sample for SEM (Fig. 3). The cross sections revealed that some of the larger particles were hollow.

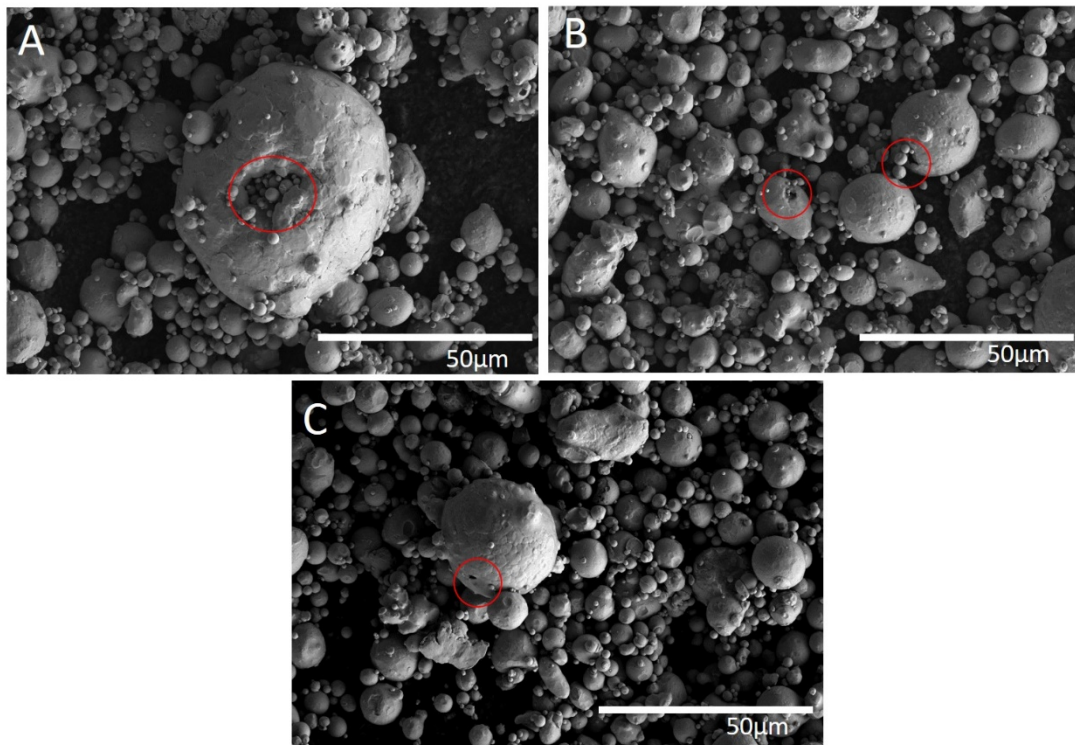


Fig. 1 SEM micrographs of the as-atomized powder. The circled regions show porosity in the powder, indicating hollow powder particles.

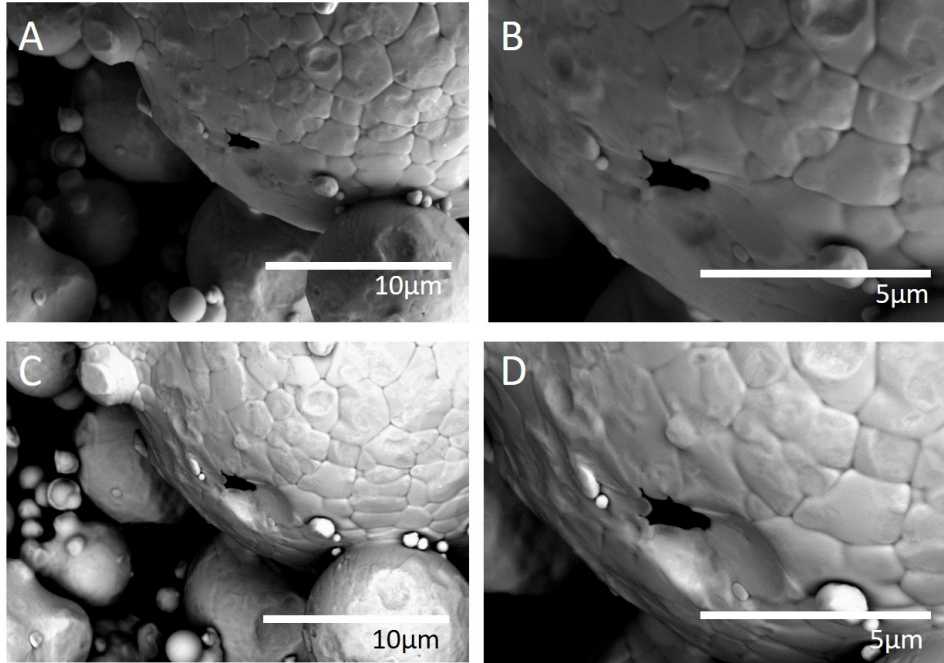


Fig. 2 High-magnification micrographs in secondary a and b) and backscatter c and d) of the pore circled in Fig. 1c

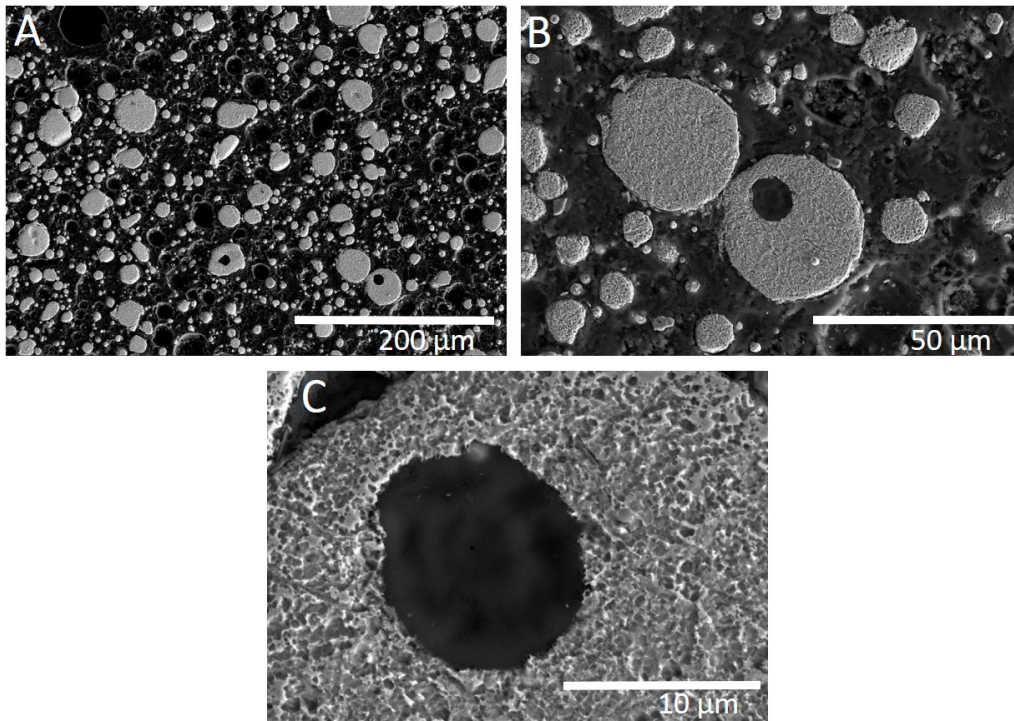


Fig. 3 Cross sections of powder samples showing a powder pore and hollow particle

The Camsizer X2 was used to quantify the PSD and sphericity of the powder (Fig. 4 and Table 1). The PSD curve (Fig. 4a) shows that the large (potentially) hollow particles make up a small percentage of the powder particles. The micrographs (Figs. 1 and 2) show that the larger particles tend to be less spherical than the smaller particles and have more satellites. The sphericity curve (Fig. 4b) does not show a correlation between particle size and sphericity, but does indicate that the powder has an average sphericity of 0.75 (a sphericity of 1 would indicate a perfect sphere). The Camsizer also calculated an average symmetry of 0.91 (Table 1) (a value of 1 would indicate perfect symmetry).¹⁶ These morphological values are indicative of a good powder for L-PBF.²⁻⁶

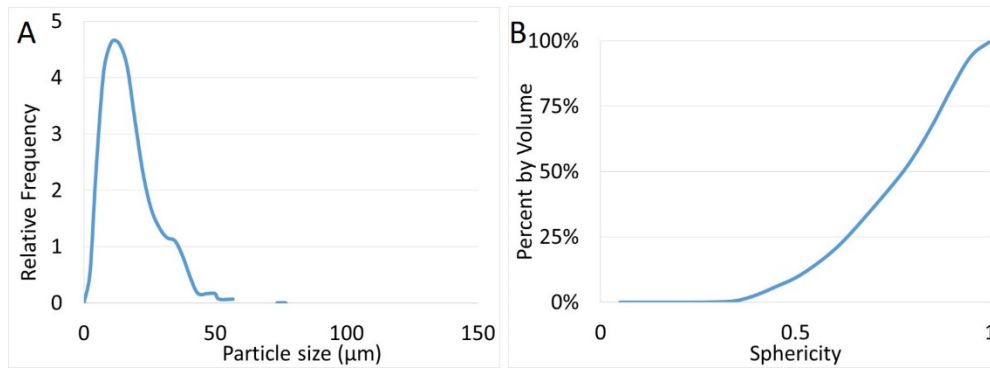


Fig. 4 Particle size distribution a) and sphericity b) measurements for the as-received powder

Table 1 PSD and morphology measurements for the as-received, cryomilled, and cryomilled and degassed powders

| Powder | D10 (µm) | D50 (µm) | D90 (µm) | Mean average sphericity | Mean average symmetry |
|----------------------------------|----------|----------|----------|-------------------------|-----------------------|
| As-atomized (sieved) | 6.38 | 15.27 | 32.16 | 0.74 | 0.91 |
| As-cryomilled | 10.98 | 27.50 | 72.22 | 0.66 | 0.89 |
| Cryomilled and degassed (sieved) | 10.13 | 21.41 | 40.19 | 0.66 | 0.89 |

The morphology of the powder greatly changed after cryomilling (Fig. 5). Figure 5 consists of micrographs of the as-cryomilled powder (a and b) and of the cryomilled, degassed, and sieved powder (c and d). After 2 h of cryomilling the powder is no longer spherical and is shaped like thin plates. The PSD for the cryomilled powder shows that there are more large particles than in the as-received

powder due to the agglomeration of fines from cold welding during milling (Fig. 6a, Table 1). After degassing, the largest powders were sieved out with a -325 mesh to prepare the powder for use in L-PBF.

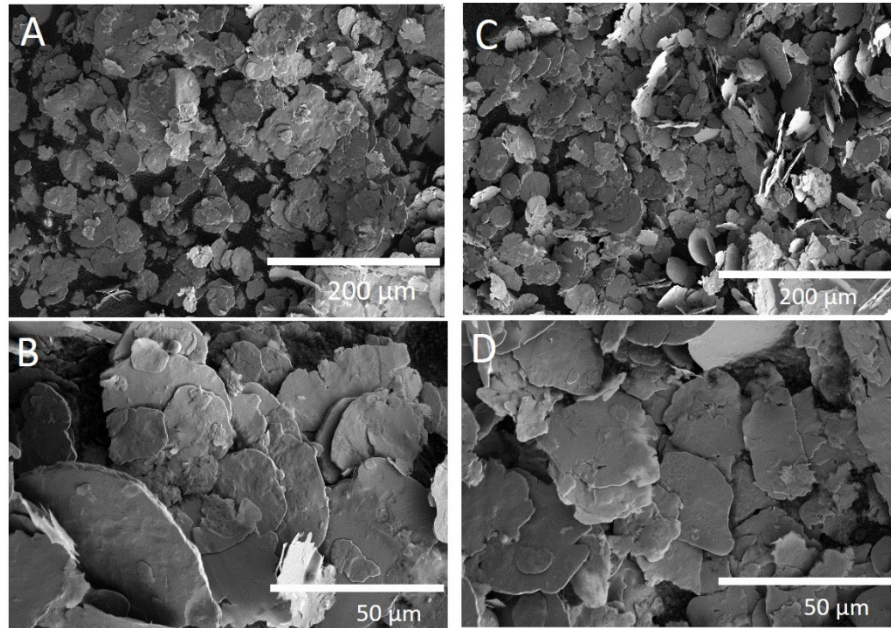


Fig. 5 SEM micrographs: 2-h cryomilled powder a and b); 2-h cryomilled, degassed, and sieved powder c and d)

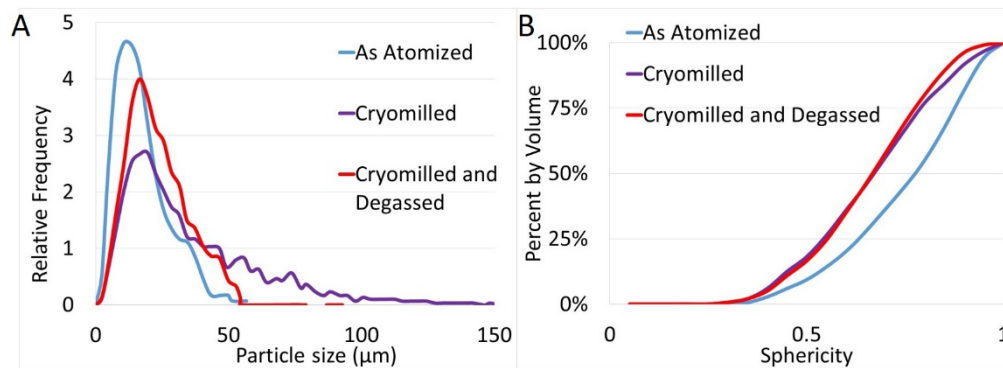


Fig. 6 PSD a) and morphology measurements b) of the 2-h cryomilled powder and of the 2-h cryomilled, degassed, and sieved powder with the as-received powder

There appears to be a discrepancy between the degree of morphological change as seen in the SEM micrographs (Fig. 5) and as measured by the Camsizer (Fig. 6b and Table 1). The Camsizer measurements indicate only a small change in morphology as the average sphericity decreased to 0.66 from 0.74 and the average symmetry dropped to 0.89 from 0.91. The reason for this apparent discrepancy is

because the Camsizer makes sphericity measurements based off 2-D images captured by the Camsizer.¹⁶

Because of this 2-D versus 3-D situation, if a plate-like particle falls in front of the camera with the flat face facing the camera, it is measured as a symmetrical sphere (Fig. 7). The Camsizer has a resolution of between 1 and 2 μm ; therefore, if a particle falls in front of the camera on edge, it is likely to be below the resolution of the camera and will not be captured and measured. This artificially makes the powder look more spherical than it is by not measuring the particles that fall on edge.

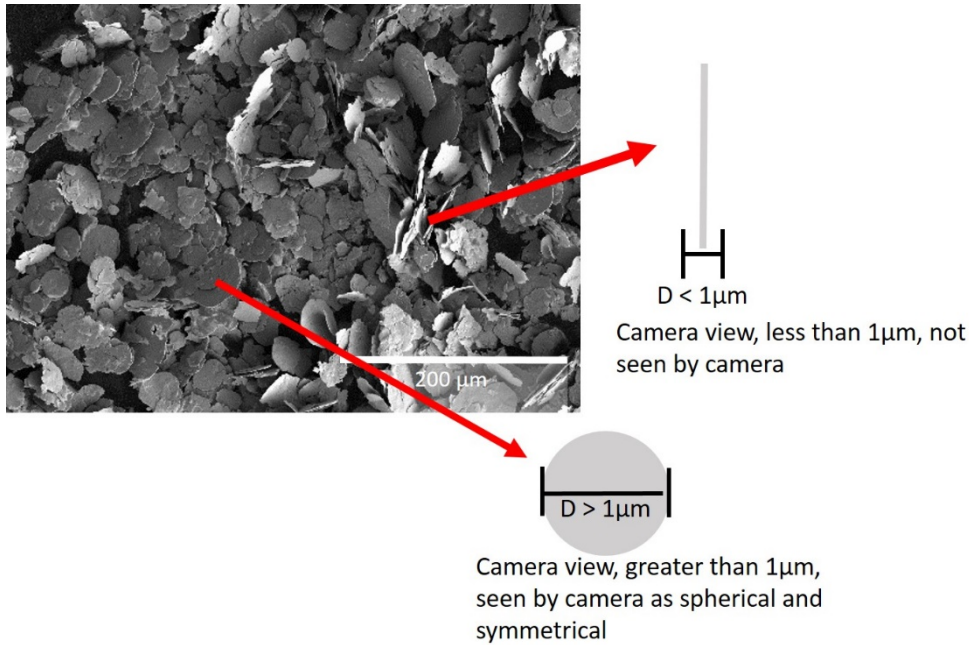


Fig. 7 Schematic demonstrating the measurement limitations of the Camsizer, which would bias the sphericity results due to the morphological changes after cryomilling

Neither the SEM (Fig. 5) nor the Camsizer (Fig. 6b and Table 1) show any morphological differences that can be linked to the degassing process. XRD measurements showed that neither cryomilling nor degassing processes induced any phase changes (Fig. 8).

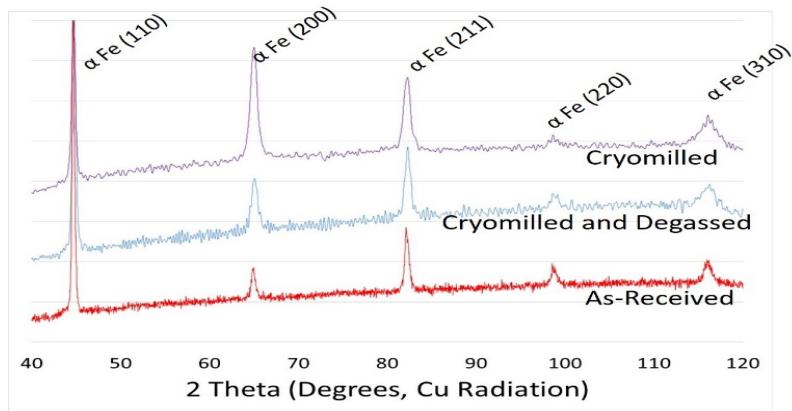


Fig. 8 XRD patterns of the 17-4 powders used in this study

Degassing was used to remove stearic acid added as a PCA. TGA measurements (Fig. 9a) show that stearic acid begins to decompose and lose mass by 250 °C and is completely gone by 400 °C. Powder was degassed at 325 °C for 6 h to remove the stearic acid without inducing any phase changes. Neither TGA (not included here) nor DSC measurements (Fig. 9b and c) could detect the presence or removal of stearic acid from the cryomilled powder, most likely due to the small amount of stearic acid used as a PCA (0.15 wt%).

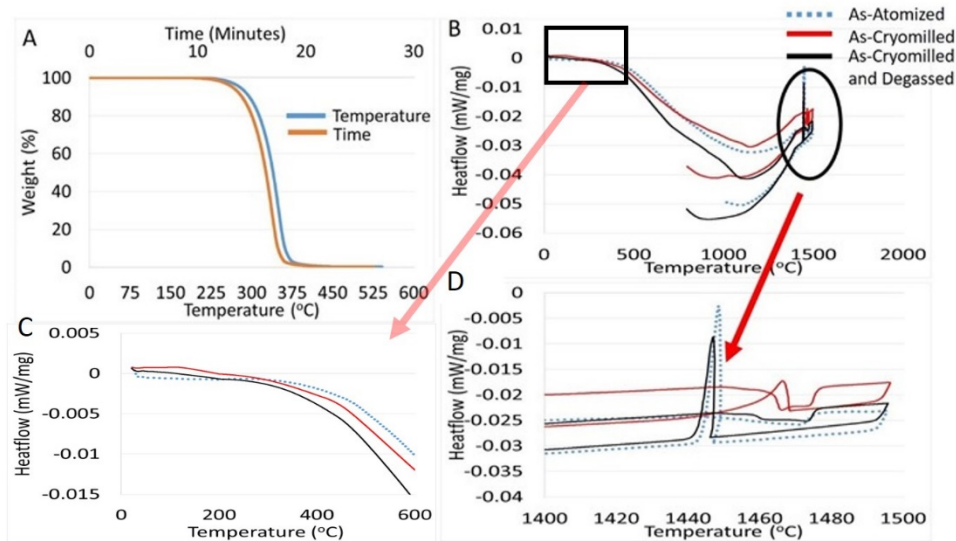


Fig. 9 TGA curve of stearic acid a) and DSC curves b) of the powders showing no difference between the thermal behaviors of the powders. c) Temperature regime over which stearic acid would be found. d) Melting and solidification portions of the curve. Exotherm up in b, c, and d with a 5 °C/min heating rate.

The XRD and DSC measurements show no differences between the as-received and the cryomilled and degassed powders (it is not clear why the melting peak for the as-cryomilled powder shifts relative to the other powders in Fig. 9c, Table 2). The only observed changes appear to be morphological.

Table 2 Melting and solidification values from DSC measurements

| Melting/Solidification | Temperature (°C) |
|---|-------------------------|
| Literature melting range ^a | 1404–1440 |
| As-atomized powder melting range | 1448–1473 |
| As-cryomilled powder melting range | 1463–1476 |
| Cryomilled, degassed, and sieved melting range | 1458–1473 |
| As-atomized powder solidification point | 1450 |
| As-cryomilled powder solidification point | 1468 |
| Cryomilled, degassed, and sieved solidification point | 1448 |

^a Sandmeyer Steel Company. Specification sheet: alloy 17-4PH (UNS S17400) W. Nr. 1.4542 type 630. Philadelphia (PA): Sandmeyer Steel Company. [accessed 2020 Apr 21]. <https://www.sandmeyersteel.com/images/17-4ph-spec-sheet.pdf>.

Brookfield powder flow testers measure the force needed to consolidate a powder into a packed powder bed (the major principle consolidation stress) and the shear force needed to make the powder achieve steady-state flow (the unconfined failure stress). These stresses can be plotted, along with generic values representing cohesive and free-flowing powders, to provide an indication of whether the powder will spread easily. The cryomilled and degassed powder is slightly more free-flowing than the as-atomized powder (Fig. 10). This is an unexpected result, as spheres should be more free-flowing than plates. The improved flow may be attributable to the removal of the finest particles in the as-received powder during the cryomilling process (Fig. 6 and Table 1).⁹ The cryomilling process also removed all satellites, which are known to reduce powder flow.⁹ It is unclear how much of the change in powder flow is related to this change in the PSD, the change in morphology, or the change in the surface chemistry of the particles through both the cryomilling and degassing processes. Alternatively, the improved flow may be an artifact of the test method. Further investigation into these relationships and flow test methods are warranted but are not part of this study.

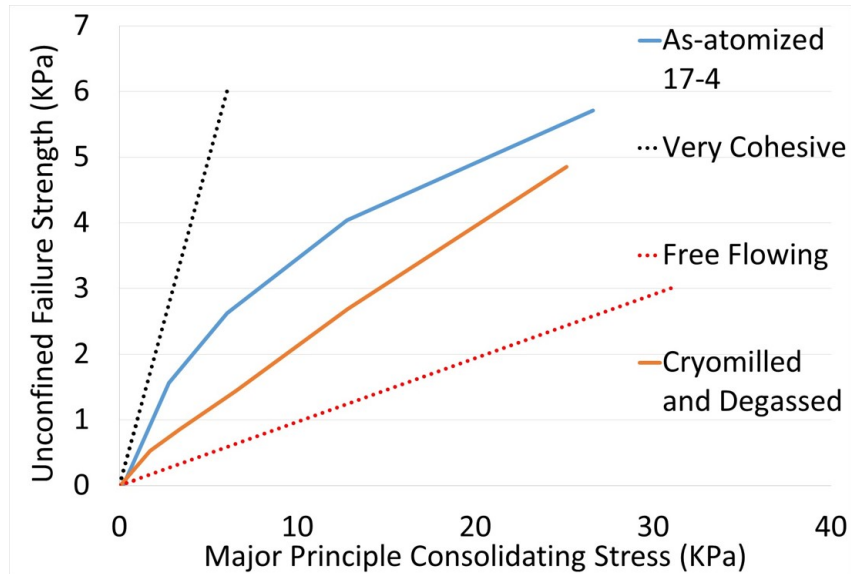


Fig. 10 Brookfield powder flow results

The cryomilled and degassed powder was used as feedstock for a 3-D systems ProX 100 to make 6-mm-diameter by 10-mm-tall cylinders (Fig. 11). It was observed during the L-PBF process that the powder was flowing within the chamber much more readily than under normal circumstances. The pressure exerted by the laser beam constantly stirred up the powder creating issues with powder coverage. This aided in the resulting parts being very porous.

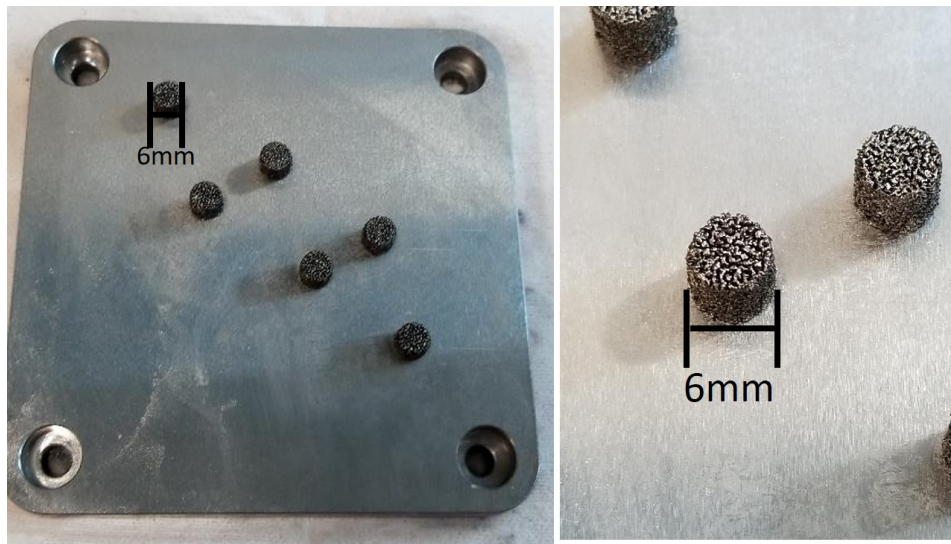


Fig. 11 Cylinders produced via L-PBF with cryomilled and degassed powder

The μ CT scans (Figs. 12 and 13) indicated that the cylinders were 60% dense. The open porosity was calculated as approximately 35% of the volume (the open porosity calculation may be under represented because it was a 3-D calculation

from 2-D measurements). The μ CT scans along the build direction (Fig. 12) appeared to show that the porosity was continuous throughout the build. Along the diameter of the sample (Fig. 13), continuous pores from one end of the sample to the other (open porosity) are evident along with sealed pores. Mechanically, the cylinders were not tested but are assumed to have very low mechanical properties due to the large amount of porosity.

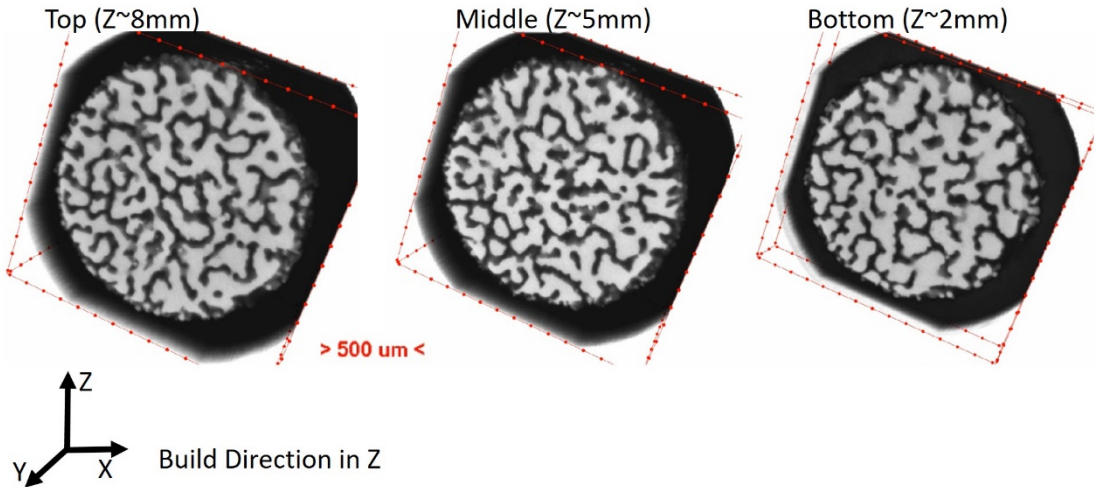


Fig. 12 μ CT slices along the build direction (length) of the cylinders

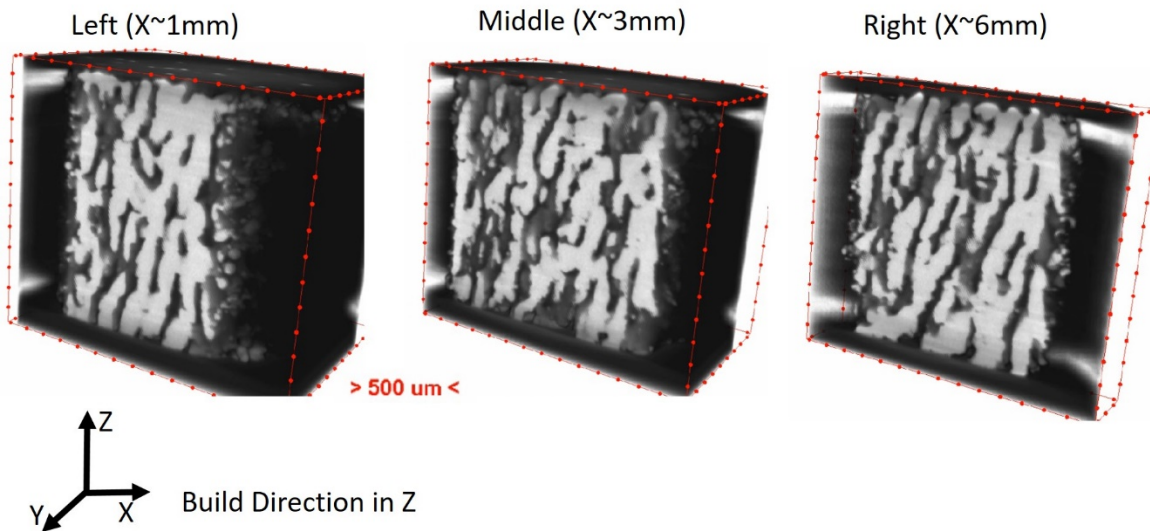


Fig. 13 μ CT slices along the diameter (X-direction) of the cylinders

4. Conclusion

In this study, 17-4 SS powder was cryomilled for 2 h to show whether cryomilling could be used to develop feedstock for L-PBF AM processes. The morphological changes of the cryomilled powder, when processed under the same L-PBF parameters as the as-atomized powder, led to the production of porous, almost foam-like cylinders. The morphological changes led to a pore- and satellite-free powder with improved flow but also lowered the packing density of powder (plates do not pack as well as spheres).¹⁰ The improved flowability and decreased packing led to the inability to maintain a proper powder bed during processing.

There are two potential paths that could be followed to improve the processability of the cryomilled powders during L-PBF. The first path would be to optimize the processing parameters of the AM machine (e.g., scan speed, laser power, and hatch spacing) for the cryomilled powder. A slower scan speed at the same laser power would increase energy density while decreasing the pressure exerted on the powder, decreasing the amount of powder blowing around within the build chamber, and improving powder coverage across the build. The increased energy density from the slower scan speed (also achievable with a higher laser power) may also be needed to handle the (potentially) higher reflectivity of the cryomilled powder (due to the increased powder surface area after milling). Increasing the layer thickness could also help improve powder coverage. The improvements in performance from changing AM processing parameters may lead to improvements, but the plate like nature of the powder may still lead to higher porosity relative to a well-atomized powder.

The second improvement path is to change cryomilling procedures to prevent the formation of the plate morphology. This could be accomplished by changing the size of the milling media. Smaller media would do less milling work on the powder and lead to a less plate-like powder. However, smaller media might not impart enough energy on the particles to remove particle porosity. Multiple cryomilling runs with different media sizes may be needed to properly remove particle porosity while maintaining particle sphericity. Another change would be to mill for longer times. Studies with aluminum show that the powder morphology changes from spherical to plate-like to roughly spherical during an 8-h cryomill run.¹³ Unfortunately, there is some evidence with 316L SS that this may not be the case when cryomilling SS powders.¹⁷ A posttreatment after cryomilling via plasma spheroidization could be used to make the powder spherical but might reintroduce porosity to the powder.

Cryomilling may be a viable process for producing SS AM powder feedstock material. However, more work needs to be done to correlate particle morphology to milling parameters to ensure the final powder is in a shape that lends itself to the AM process.

5. References

1. Kudzal A, McWilliams B, Hofmeister C, Kellogg F, Yu J, Taggart-Scarff J, Liang J. Effect of scan pattern on the microstructure and mechanical properties of powder bed fusion additive manufactured 17-4 stainless steel. *Materials and Design*. 2017;133:205–215. doi: <http://dx.doi.org/10.1016/j.matdes.2017.07.047>.
2. Zhang Y, Wu L, Guo X, Kane S, Deng Y, Jung Y, Lee J, Zhang J. Additive manufacturing of metallic materials: a review. *Journal of Engineering Materials and Performance*. 2018;27(1):1–13. doi: <https://doi.org/10.1007/s11665-017-2747-y>.
3. Mower T, Long M. Mechanical behavior of additive manufactured, powder-bed laser-fused materials. *Materials Science and Engineering A*. 2016;651:198–213. doi: <http://dx.doi.org/10.1016/j.msea.2015.10.068>.
4. Adeyemi A, Akinlabi ET, Mahmood R. Powder bed based laser additive manufacturing process of stainless steel: a review. *Materials Today: Proceedings*. 2018;(5):18510–18517.
5. Anderson I, White E, Dehoff R. Feedstock powder processing research needs for additive manufacturing development. *Current Opinion in Solid State and Materials Science*. 2018;22:8–15. doi: <https://doi.org/10.1016/j.cossms.2018.01.002>.
6. Aboulkhair N, Simonelli M, Parry L, Ashcroft I, Tuck C, Hague R. 3-D printing of aluminium alloys: additive manufacturing of aluminium alloys using selective laser melting. *Progress in Materials Science*. 2019;106:1–45. doi: <https://doi.org/10.1016/j.pmatsci.2019.100578>.
7. Bumiller M. The importance of particle shape. Technical note. [accessed 2020 Mar 23]. <https://www.horiba.com/scientific/products/particle-characterization/download-center/webinars/tr017/>.
8. Leturia M, Benali M, Lagarde S, Ronga I, Saleh K. Characterization of flow properties of cohesive powders: a comparative study of traditional and new testing methods. *Powder Technology*. 2014;253:406–423. doi: <http://dx.doi.org/10.1016/j.powtec.2013.11.045>.
9. Goh H, Heng P, Liew C. Comparative evaluation of powder flow parameters with reference to particle size and shape. *International Journal of Pharmaceutics*. 2018;547:133–141. doi: <https://doi.org/10.1016/j.ijpharm.2018.05.059>.

10. German R. Particle packing characteristics. Princeton (NJ): Metal Powder Industries Federation; 1999.
11. Meredith S, Zuback J, Keist J, Palmer T. Impact of composition on the heat treatment response of additively manufactured 17-4PH grade stainless steel. *Materials Science and Engineering A*. 2018;738:44–56. doi: <https://doi.org/10.1016/j.msea.2018.09.066>.
12. Lass E, Zhang F, Campbell C. Nitrogen effects in additively manufactured martensitic stainless steels: conventional thermal processing and comparison with wrought. *Metallurgical and Materials Transactions A*. 2020;51A:2318–2332. DOI: <https://doi.org/10.1007/s11661-020-05703-6>.
13. Kellogg F, Hofmeister C, Giri A, Cho K. Nanostructuring of aluminum alloy powders by cryogenic attrition with hydrogen-free process control agent. Aberdeen Proving Ground (MD): Army Research Laboratory (US); 2015 Feb. Report No.: ARL-TR-7208.
14. Witkin D, Lavernia E. Synthesis and mechanical behavior of nanostructured materials via cryomilling. *Progress in Materials Science*. 2006;51(1):1–60.
15. Kellogg F, McWilliams B, Sietins J, Giri A, Cho K. Comparison of SPS processing behavior between as atomized and cryomilled aluminum alloy 5083 powder. *Metallurgical and Materials Transactions A*. 2017;48a:5492–5499. doi: 10.1007/s11661-017-4286-4.
16. Understanding the Shape Parameters Reported by the CAMSIZER. Horiba Technical Note 164 (TN164). [accessed 2020 Apr 16]. <https://www.horiba.com/scientific/products/particle-characterization/download-center/technical-notes/>.
17. Lau ML, Lavernia EJ. Microstructural evolution and oxidation behavior of nanocrystalline 316-stainless steel coatings produced by high-velocity oxygen fuel spraying. *Materials Science and Engineering A*. 1999;272(1):222–229.

List of Symbols, Abbreviations, and Acronyms

| | |
|----------|-----------------------------------|
| μ CT | X-ray microcomputed tomography |
| 3-D | three-dimensional |
| AM | additive manufacturing |
| DSC | differential scanning calorimetry |
| L-PBF | laser powder bed fusion |
| PCA | process control aid |
| PSD | particle size distribution |
| SEM | scanning electron microscopy |
| SS | stainless steel |
| TGA | thermogravimetric analysis |
| XRD | X-ray diffraction |

1 DEFENSE TECHNICAL
(PDF) INFORMATION CTR
DTIC OCA

1 CCDC ARL
(PDF) FCDD RLD CL
TECH LIB

7 CCDC ARL
(PDF) FCCD RLW MD
F KELLOGG
A KUDZAL
C MOCK
J TAGGART-SCARFF
R ROGERS
B MCWILLIAMS
K CHO